A Computational Study of a Supersonic Mixer-Ejector Exhaust System

T. J. Barber

United Technologies Research Center, East Hartford, CT

November 10, 1992

R92-957930

Contents

St-A per telecon, Mr. Shreeve,
Naval Postgraduate School/Code 67SF.
Monterey, CA 93943

JK 12-8-92

List of Tables

List of Figures

Nomenclature

A_s	Ejector secondary area (in^2)
A_p, A_e	Ejector primary area (nozzle exit area) (in^2)
AR	Ejector area ratio (A_3/A_P)
A_3	Ejector mixing duct area (in^2)
B	Slot-nozzle width (long dimension) (in)
C_p	Specific heat ($ft^2/sec^2/°R$)
g	Gravitational constant
H_E	Ejector shroud exit height (in)
H_T	Total enthalpy (ft^2/sec^2)
h	Slot nozzle height (short dimension) (in)
h_1, h_2, h_3	Metric or grid scale factors
$\dot{H}_T$	Enthaply flux ($ft\ lbf/sec$)
L	Length of ejector shroud (in)
L_d	Length of ejector mixing duct (in)
M	Local flow Mach number
M_∞	Forward flight Mach number
M_J	Jet exit Mach number
$\dot{m}_s$	Ejector secondary weight flow (lbm/sec)
$\dot{m}_p$	Ejector primary weight flow (lbm/sec)
$\dot{m}$	Total integrated mass flow (lbm/sec)
NPR	Nozzle pressure ratio ($P_{TJ}/P_{S\infty}$)

P	Static pressure ($psia$)
P_T	Flow field total pressure ($psia$)
R	Gas constant ($ft^2/sec^2/°R$)
S	Entropy ($ft^2/sec^2/°R$)
T	Static temperature ($°R$)
T_T	Flow field total temperature ($°R$)
$\dot{T}$	Stream thrust (lbf)
U_1, U_2, U_3	Velocity components (ft/sec)
$\bar{U}$	Fully mixed flow velocity (ft/sec)
W_E	Ejector shroud exit width (in)
X_p	Axial penetration of nozzle exit plane into ejector shroud (in)
X *or* Y_1	Axial distance (in)
Y *or* Y_2	Transverse distance (in)
Z *or* Y_3	Vertical distance (in)
γ	Ratio of specific heats
λ	Heat conductivity ($ft\ lbf/ft/sec/°R$)
Ω	Streamwise component of vorticity
μ	Viscosity ($slug/ft/sec$)
ρ	Density ($slugs/ft^3$)

Subscripts:

$J, P, 1$	Primary, nozzle exit or jet flow state
∞	Wind tunnel freestream or ambient flow state
s	Secondary flow state
$*$	Sonic flow state

Superscripts:

$-$	Average condition

1 Abstract

An analytical model of the mixer ejector based on a PNS solver approach has been applied to analyze the flowfield downstrean of a supersonic mixer-ejector exhaust system. The method has been used previously to analyze the plume flowfield of unshrouded mixer-type nozzles as well as the flowfield within the mixing duct of a mixer-ejector exhaust system. Calculations are presented for a model-scale exhaust system operating at takeoff flight conditions. Favorable comparisons with total temperature and pressure experimental data are presented in the text. In addition parametric studies are presented examining the importance of turbulence level, streamwise vorticity, grid resolution, etc. on the downstream plume mixing characteristics. Finally, a series of calculations examining the effect of engine power setting (operating condition) and exhaust system size (full scale) are analyzed.

2 Background

A three-dimensional viscous flow analysis has been developed and applied by Anderson and Barber in a joint analytical / experimental program [1], [2], [3] to analyze the exhaust jets produced by complex supersonic nozzles. The parabolic fully viscous method presented is an extension of a two dimensional method presented by Anderson [4] which was later extended to three dimensions by Anderson and Hankins [5] but restricted to orthogonal coordinates. In this method, the primary flow equations, which include the streamwise momentum, transverse pressure, and energy equations, are solved first for the streamwise velocity, static pressure, and total enthalpy assuming that the crossflow velocities are known. With the primary flow variables known, the secondary flow equations, which include the continuity, vorticity, and vorticity transport equation, are solved for the secondary flow variables which are the streamwise component of vorticity, and the two cross flow velocity components. The method has also been modified and applied to analyze the flowfield within the mixing duct of the ejector [6]. The ejector analysis procedure combines empirical data obtained from previous analytical/experimental studies with the PNS technique. Computational studies have been reported for a flat plate shroud, flight-inlet ejector, containing either a mixer or a slot nozzle operating at an exit Mach number of *1.5*.

3 Ejector Plume Analysis Approach

In the previously conducted ejector analysis studies, the flow field within the mixing duct or internal flow portion of the exhaust system is controlled by the mixed-out exit static pressure and the nozzle exit flow field. Therefore, the PNS-based analysis, which required input parameters to initialize the

calculation, resorted to a combination of experimental and empirically determined parameters at the starting plane of the calculation. For example, internal flow calculations have been performed (see Appendix) where the experimentally determined pumping rate was specified and the equilibrium jet approximation imposed ($P_s = P_J$) in lieu of specifiying the ejector exit static pressure to drive the pumping. In those calculations, the nozzle exit or jet (J) conditions have been assumed to exhibit the same distributional characteristics as measured in the unshrouded mixer nozzle program [2]. The specific level of induced exit plane vorticity (Ω_{max}), however, has to be empirically determined from the experimental levels of pumping. Experience in setting this parameter and validation of the internal flow model has been obtained by performing calculations on mixer-ejector configurations previously studied experimentally at UTRC.

In the current analytical effort, the experimental P_{TJ}, T_{TJ}, and Ω (determined from U_2, U_3 LV data) are combined with the freestream or coflowing conditions to generate the starting plane profile. The P_T and T_T data are then normalized using the following relation,

$$\overline{F} = \frac{F - F_\infty}{F_J - F_\infty} \tag{1}$$

where the subscript (J) refers to the jet (primary) conditions, and the subscript (∞) refers to the free stream (secondary) conditions. In this format, the flow conditions can be rescaled to the test conditions.

The initial cross flow velocity components U_2, U_3 are also very important because they determine the magnitude of the enhanced mixing. These cross plane velocities were determined in an indirect manner since the analysis requires as input the streamwise component of the vorticity $\Omega(Y_2, Y_3)$ and then solves the Cauchy-Riemann problem given by,

$$\frac{\partial U_2}{\partial Y_2} + \frac{\partial U_3}{\partial Y_3} = 0 \tag{2}$$

$$\frac{\partial U_3}{\partial Y_2} - \frac{\partial U_2}{\partial Y_3} = \Omega \tag{3}$$

The external or plume portion of the calculation is performed over a domain of sufficient lateral and axial extent so as to capture the mixing of the jet to ambient conditions. This calculation can be initialized using the exit flow field from the internal calculation and the ambient coflowing stream. A shear layer is constructed based on a nominal flat plate boundary layer growth along

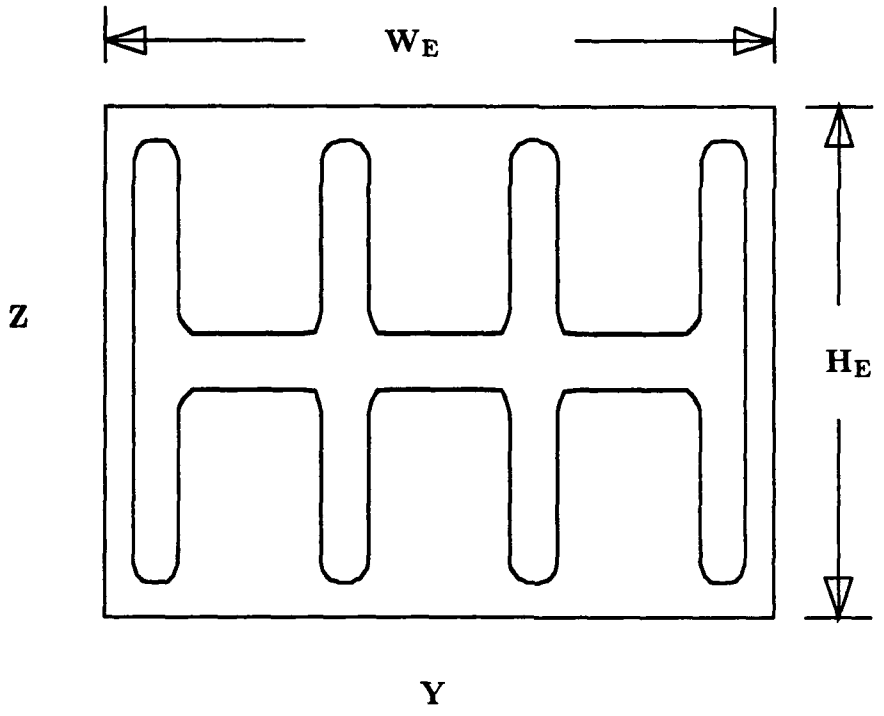

Figure 1: End View of Advanced Mixer Ejector

both surfaces of the ejector wall. In situations where experimental data was obtained at the ejector exit plane, P_T, T_T profiles are used in conjunction with the analytically determined cross-flow field.

3.1 Geometry and Grid Issues

A schematic of the mixer ejector exhaust system is shown on Figs. 1 and 2 showing the end view and side view respectively. The end view, shown in Fig. 1, has an outline of the advanced mixer exhaust nozzle surrounded by a rectangular shroud of width W_E and height H_E. The side view shown on Fig. 2 shows the advanced mixer exhaust nozzle exit plane at $X/L = -1$ surrounded by a shrouded duct of length L. The current computational simulations were started at the ejector exit plane.

The exhaust plume calculations were conducted using a Cartesian grid. All calculations performed

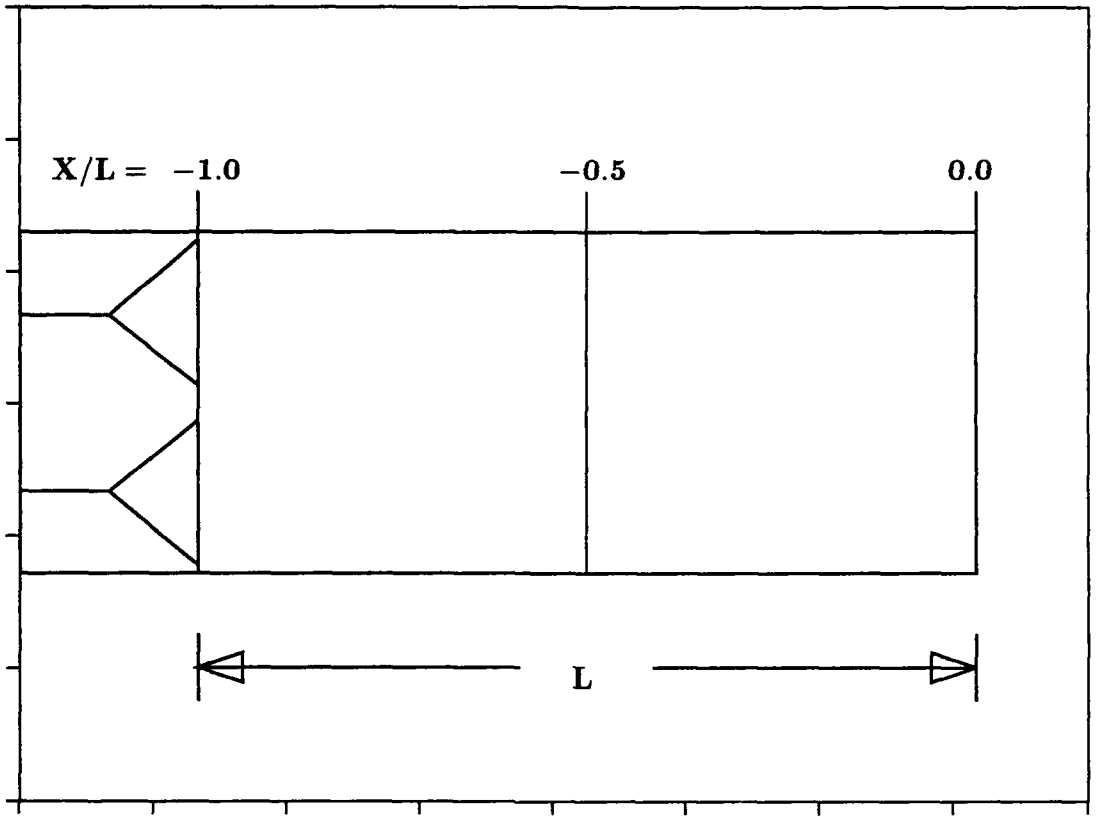

Figure 2: Side View of Advanced Mixer Ejector

in this study assumed a 1/4 plane symmetry. The external calculations used a (99 by 99) cross-planar grid composed of uniform inner grid (80 by 80) in conjunction with a outer grid stretched geometrically to the freestream or coflowing boundary so as to avoid influencing the plume mixing rate. In this inner region the grid spacing, referenced to the mixer nozzle effective hydraulic diameter, is approximately *0.027*, or about 22 points per mixer lobe. The axial mesh was also geometrically stretched to allow for a more gradual evolution of the turbulent jet flow. Approximately 175 axial planes were used over the first 10 feet of the jet. Parametric mesh studies involving cross-planar meshes ranging from (50 by 50) to (120 by 120), have demonstrated that (99 by 99) point meshes accurately model the ejectors mixing characteristics. As a side note on computational efficiency, a comparison was made for a typical internal calculation, involving approximately 300,000 grid points (50 by 50 cross-planar mesh) which required about 1.5 hours on a CRAY XMP. It should be noted that an equivalent calculation [8], using a pressure-correction based Navier-Stokes scheme, required 26 CRAY XMP CPU hours. An approximately 20 to 1 speed up definitely qualifies the

PNS approach as efficient; the calculation/ experiment comparisons below will demonstrate the effectiveness of the method.

3.2 Flow Boundary Conditions

In the current analytical study, experimental flow conditions are interpolated onto the computational grid at the ejector exit plane, with additional flow field definition obtained by extrapolating from the edge of the experimental data domain to coflowing or far field conditions. Traverse mesh densities were typically (28 by 18) over the 1/4 plane for (P_T, T_T) and (14 by 10) over the 1/4 plane for the velocity field. The PATH code requires streamwise vorticity input, rather than U_2, U_3, therefore Ω_s was determined using second order accurate differencing of the experimental data. A maximum value of $\Omega_s \approx 6000$ per second was measured for the AR = 4.0 ejector case (only case where LV data obtained). All vector components normal to planes of symmetry were zeroed out for consistency with 1/4 plane of symmetry calculation. Color plots of the normalized (T_T, P_T) and Ω_s) data are shown in Fig. 3. Note the strong residual effect of the mixer nozzle central core, cited in Ref. [6], and the modest alignment of the vorticity "cells" with the superimposed upstream mixer nozzle lobe side walls.

4 Discussion of Computational Results

Calculations for the AR = 4.0 ejector configuration were obtained and compared with experimental (P_T, T_T) data at three planes located approximately *3.3, 10.3* and *40.3* inches downstream of the ejector exit plane. When referenced to the nozzle effective hydraulic radius, these planes are *2.04, 6.4* and *24.9* units from the ejector exit. A more meaningful measure, however, is from the mixer nozzle exit plane. Since the normalized ejector length is *6.5*, the traverse planes are located *8.5, 12.9* and *31.4* units from the nozzle exit. The comparisons with experimental data are shown in terms of color contours in Figs. 4, 5, and 6. The color bar for the contour plots has been doubly expanded to highlight the comparisons as the exhaust flow approaches free stream or coflowing conditions. Note both analysis and experiment predict the rapid decay of exhaust flow from the lobe region of the nozzle, as well as the slow decay rate of the central core. In fact, the central core decays in a manner similar to a slot nozzle. Additional calculations obtained beyond the last experimental traverse plane show that the slot eventually decays to the expected round jet in the far field. Computational studies presented in the Appendix and in Ref. [6] have demonstrated that the central core arises from inability of the induced secondary flow to penetrate the four cross-flow nozzle centerline stagnation regions. A crossflow stagnation point arises when the nozzle centerline intersects each mixer lobe bisector. The four lobe nozzle configuration therefore produces the four

"bulls-eye" regions seen in Figs 4, 5, and 6. Figure 7 also shows a comparison of the centerline decay of the normalized total temperature for both the experimental and computational results. Good agreement is noted for the limited data available. Closer study notes that the rapid initial decay reaches a plateau region and is eventually passed by the faster farfield decay rate of the more conventional slot ejector configuration. The presence of the plateau region will be explored in more detail in the assessment of a full-scale configuration.

4.1 Parametric studies

The comparisons of the PATH PNS analysis with experimental data have been used to validate the computational approach. The analysis can therefore be now used to explore the dependence of a number of key physical and numerical parameters on the rate of plume mixing.

Grid density study: One aim of the present study is to perform mixing effectiveness studies on the exit plume. This required a complete flow field definition, specified sufficiently far downstream so that the warmest region of the flow was only 10% from the freestream total temperature level ($\overline{T_T}$ = .05). This level occured approximately 320 diameters downstream of the exit plane. In an attempt to minimize the PATH code computational run time for such an extended domain, a solution on a coarser 50 by 50 mesh case was calculated and compared to the previous results (obtained on a 99 by 99 mesh). Figure 8 illustrates that at a distance of *40.3* inches (24.894), the coarse mesh jet solution already looks like a "far-field" round jet, rather than the actual slot-like jet. The enhanced mixing effect arises from the artificial viscosity introduced by the coarse mesh.

Initial turbulence level study: Since no measurements were performed to define the turbulence characteristics of the ejector exhaust flow, analytical models are typically used to provide an estimate in order to initialize CFD calculations. In the PATH code one typically uses an algebraic Prandtl mixing length model to extract the initial or ejector exit levels for the turbulence energy (k) and the turbulent dissipation (ϵ) dependent variables of the two-equation turbulence model. A more realistic estimate however was obtained by performing an internal flow calculation (from the mixer nozzle exit to the ejector exit plane), as cited in the Appendix and in Ref. [6]. While the calculation of the general flow properties is strongly dependent on an empirical model to define the initial plane of the calculation (nozzle exit profile, pumping level, etc.), the internal flow result can be used to more realistically set the exit plane turbulence level. Figure 9 shows a comparison of both types of turbulence intializations at a plane *10.3* inches (6.362) downstream of the ejector exit. The algebraic model provides too low an estimate of the exit plane turbulence level, resulting in almost no mixing over the 10.3 inches. In contrast, the internally driven estimate, shown here

and in Figure 9, produced the good comparisons with experimental data.

Streamwise vorticity study: The use of convoluted surfaces (mixer lobes) to enhance mixing levels has been demonstrated in a number of analytical and experimental studies. The reason for this enhanced mixing has been largely attributed to the generation of streamwise vorticity through the use of surface convolutions. A frequently raised objection to this concept claims that the surface convolutions simply introduce additional wetted surface area. A computational study was therefore performed to examine the impact of streamwise vorticity on jet mixing. Calculations were conducted for similar flows, differing only in the initial level of streamwise vorticity. One calculation was initialized with the measured exit streamwise vorticity distribution and one with zero streamwise vorticity. The results of these calculations are compared on Fig. 10, at a plane *10.3* inches (6.362) downstream of the ejector exit plane. Without the presence of streamwise vorticty, the plume appears to mix out as three non-interacting slot nozzles, one corresponding to the mixer nozzle center core and two corresponding to the residual effect of the lobe hot flow convected within the ejector to the upper and lower ejector walls. In addition to a different mixing history, the outer "slot nozzles" are about 10% warmer than the measured flow field. The effect of streamwise vorticity on mixing would be even more substantial if it were eliminated from the mixer nozzle exit plane rather than from the ejector exit plane. The calculations however do illustrate that enhanced mixing rates arise from the generation of streamwise vorticity.

5 Full Scale Nozzle Performance Asssessment

Having demonstrated the applicability of the PATH analysis procedure for analyzing mixing processes downstream of a model-scale mixer ejector exhaust system, one can now use the PATH code to assess the performance of a full-scale or flight-type mixer ejector configuration. If a full-scale configuration was simply a length scale L enlargement of the model-scale configuration, one must still consider what should be the corresponding modifications to the model-scale initial plane (ejector exit plane) data for a realistic simulation of the full-scale problem. The model-scale calculations in the previous section were initialized with (P_T, T_T, and Ω) data. These calculations however demonstrated that the turbulence parameters k and ϵ data also had to be specified.

While the full-scale or larger geometry implies a larger Reynolds number and probably thinner boundary layers, the total pressure and temperature data are assumed to remain unchanged in the geometrical transformation, just redistributed over the enlarged exit plane. The vorticity data however cannot remain unchanged and must be modified. If one observes that exit flow angle of

the nozzle exhaust remains the same when the mixer nozzle is enlarged by L, then U_2 and U_3 also remain unchanged. The vorticity field, defined below,

$$\Omega_{full-scale} = \frac{\partial U_3}{\partial Y_2} - \frac{\partial U_2}{\partial Y_3} = \frac{\Omega_{model-scale}}{L} \tag{4}$$

is reduced by L. In a similar fashion, one can observe that since the turbulence intensity k is proportional to u'/U_1 and that the fluctuating scales are typically unaffected by geometrical scale, k can be considered as unchanged for a full-scale simulation. On the other hand, the turbulent dissipation ϵ data must be modified. Recalling that if

$$\epsilon \approx \frac{C_\mu k^{3/2}}{L} \tag{5}$$

then $\epsilon_{full-scale}$ must be decreased by L. This also implies that the turbulent viscosity μ_T, given by

$$\mu_T \approx C_\mu \rho \frac{k^2}{\epsilon} \tag{6}$$

is correspondingly larger in the full scale problem and therefore the rate of jet mixing is increased.

A geometrical scale factor of approximately 7 was selected for resizing the model-scale nozzle to that of a typical modern fighter engine scale. Calculations for this configuration, using the PATH code, have been largely unsuccessful, primarily due to numerical instabilities arising at the shear layer interface of the ejector and free stream flows. An alternative approach was developed, wherein full Navier-Stokes (elliptic) code called NASTAR was utilized for the plume calculation. Starting conditions defined above were used to initialize a series of Navier-Stokes (NS) calculations. The NASTAR code, developed by Rhie [9], [10] is based on a control-volume pressure-correction scheme (similar to the "TEACH" code). Since the plume flow field is essentially parabolic, the axial extent was subdivided into *5* segments in order to accerelerate the numerical convergence. The computational mesh used was 75 by 75 in the crossplane, clustered near the initial ejector/free stream shear layer interface. Upstream flow conditions were selected to maintain P_T and P_∞, with T_T changes ($1000°, 1250°, 1500°$ F) specified to reflect different engine power settings. Figure 11 illustrates that the normalized centerline stagnation temperature decay, $\overline{T_T}$, shows little dependence on a 50% increase in supply temperature.

An interesting point to note about the centerline decay characteristics is the extremely long axial extent required to reach ambient conditions. A major factor leading to this feature is the plateau region established. Figure 12 illustrates the crossplane stagnation temperature field at three axial

locations in the plume, one in the initial decay region, one in the middle of the plateau region, and one at the end of the plateau region. It is readily evident that the initial rapid decay of the lobe region to the shroud walls suppresses further mixing in the vertical direction until the side wall shear layers mix inward to "circular-like" jet pattern. At this point, the plume continues to actively mix in all direction at an "effective" round jet rate.

6 Conclusions

Albeit that ejector exhaust system pumping levels are dependent on the downstream / exit pressure field and therefore any analysis should be capable of modeling the upstream interaction effects of the exit plane ambient static pressure (analysis is mathematically elliptic). The results presented in the text demonstrate however that:

- an efficient PNS based computational procedure has been developed to analyze internal and external mixing flows dominated by streamwise vorticity,
- elliptic effects can be modeled through a combination of empirical flow models and experimentally defined boundary conditions,
- predicted mixing levels as a function of ejector area ratio (AR) confirm experimentally observed levels,
- the importance of grid resolution, and initial turbulence level, i.e. (k,ϵ) on the predicted evolution of the plume has been identified, and
- the presence on an experimentally observed plateau region in the downstream region of the plume has been confirmed through analytical predictions, and the causal effect explained.

7 Acknowledgements

The author would like to thank Lou Chiappetta for his assistance on performing the calculations cited in the text. In addition, the author appreciates the assistance T. Greg Tillman and Bruce L. Morin for providing the experimental data used in the computational comparisons.

References

[1] Anderson, O. L., and Barber, T. J., "Three-Dimensional Analysis of Complex Hot Exhaust Jets," AIAA 88-3705, AIAA/ASME/SIAM/APS 1st National Fluid Dynamics Congress, July 1988.

[2] Patrick, W.P., Barber, T.J., Tillman, T.G., Anderson, O.L., and Paterson, R.W., "Experimental and Analytical Studies of Jet Mixing from Complex Supersonic Nozzles," UTRC Report R88-957270-1, Final Report for Contract N00014-85-C-0506, prepared for Department of the Navy, Naval Air Systems Command, Washington, D.C., June, 1988.

[3] Tillman, T. G., Patrick, W. P., Paterson, R. W., "Enhanced Mixing of Supersonic Jets," AIAA 88-3002, AIAA 24th Joint Propulsion Conference, July, 1988.

[4] Anderson, O. L., "Calculation of Internal Viscous Flows in Axisymmetric Ducts at Moderate to High Reynolds Numbers," Intl. J. Computers and Fluids Vol. 8, No. 4, 1980, pp. 391-411.

[5] Anderson, O. L. and Hankins, G. B., "Development of a Finite Difference Method for 3-D High Reynolds Number Viscous Internal Flows," **Computers in Flow Predictions and Fluid Dynamics Experiments**, Winter Annual Meeting ASME, November 1981, pp. 119.

[6] Barber, T. J., and Anderson, O. L., "Computational Study of a Supersonic Mixer-Ejector Exhaust System," J. of Propulsion and Power, Vol. 8, No. 5, 1992, pp. 927-934, also AIAA 91-0126, AIAA 29th Aerospace Sciences Meeting, Reno, NV, 1990.

[7] Tillman, T. G., Paterson, R. W. and Presz, W. M.. " Supersonic Nozzle Mixer Ejector," AIAA Paper AIAA-89-2925, AIAA 25th Joint Annual Propulsion Conference, July 1989.

[8] Malecki, R., and Lord, W., "Navier-Stokes Analysis of a Lobed Mixer and Nozzle," AIAA 90-0453, AIAA 28th Aerospace Sciences Meeting, Reno, NV, 1990.

[9] Rhie, C. AIAA Journal, Vol. 27, No. 8, 1989, pp. 1017-1018.

[10] Rhie, C. M., and Stowers, S. T., "Navier-Stokes Analysis for High Speed Flows Using a Pressure Correction Algorithm," AIAA J. of Propulsion and Power, Vol. 4, No. 6, 1988, pp. 564-570.

MIXER-EJECTOR CALCULATION: INITIAL CONDITIONS (EXPER.)
(A_s/A_p=4.0, M_p=0.5)

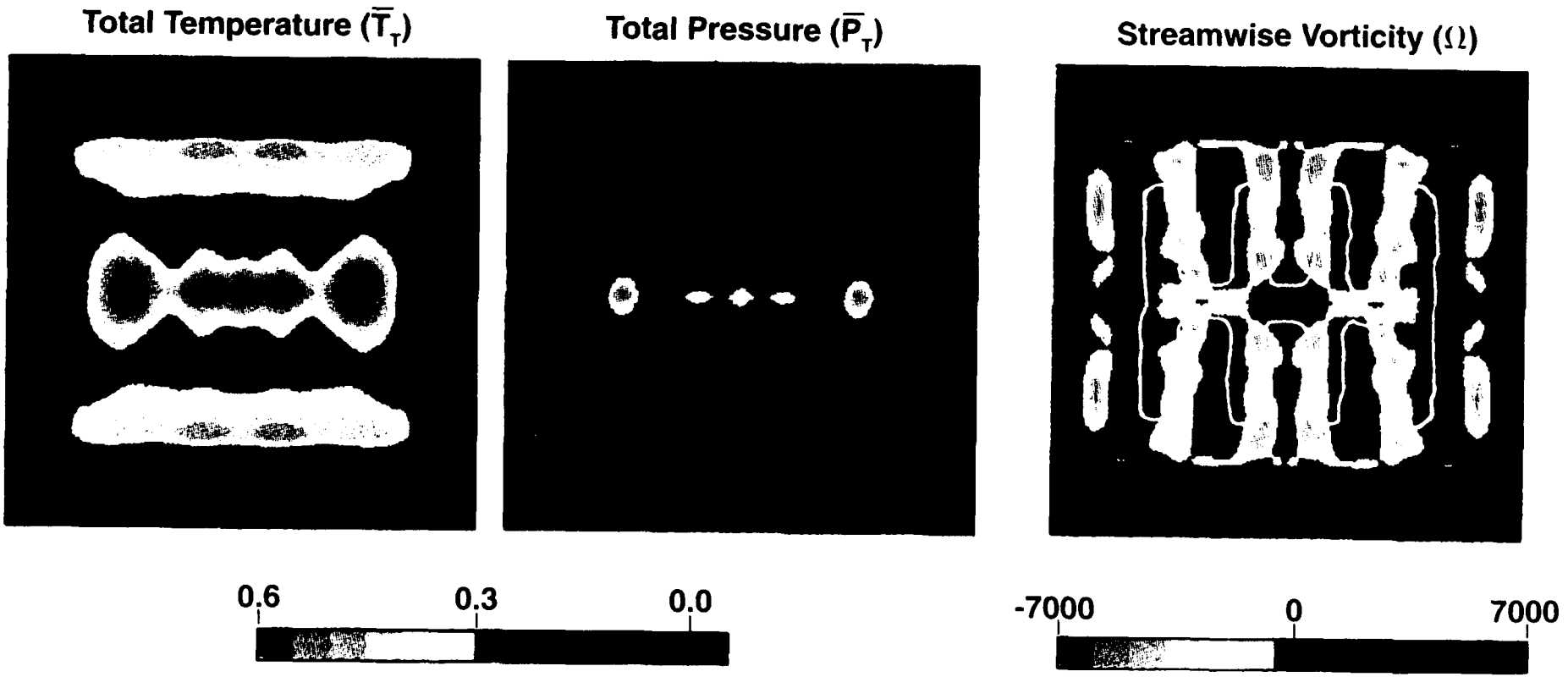

Figure 3

92-2-26-1

MIXER-EJECTOR: PLUME TOTAL TEMPERATURE: X=3.3 in.
(A_S/A_P=4.0, M_p=0.5)

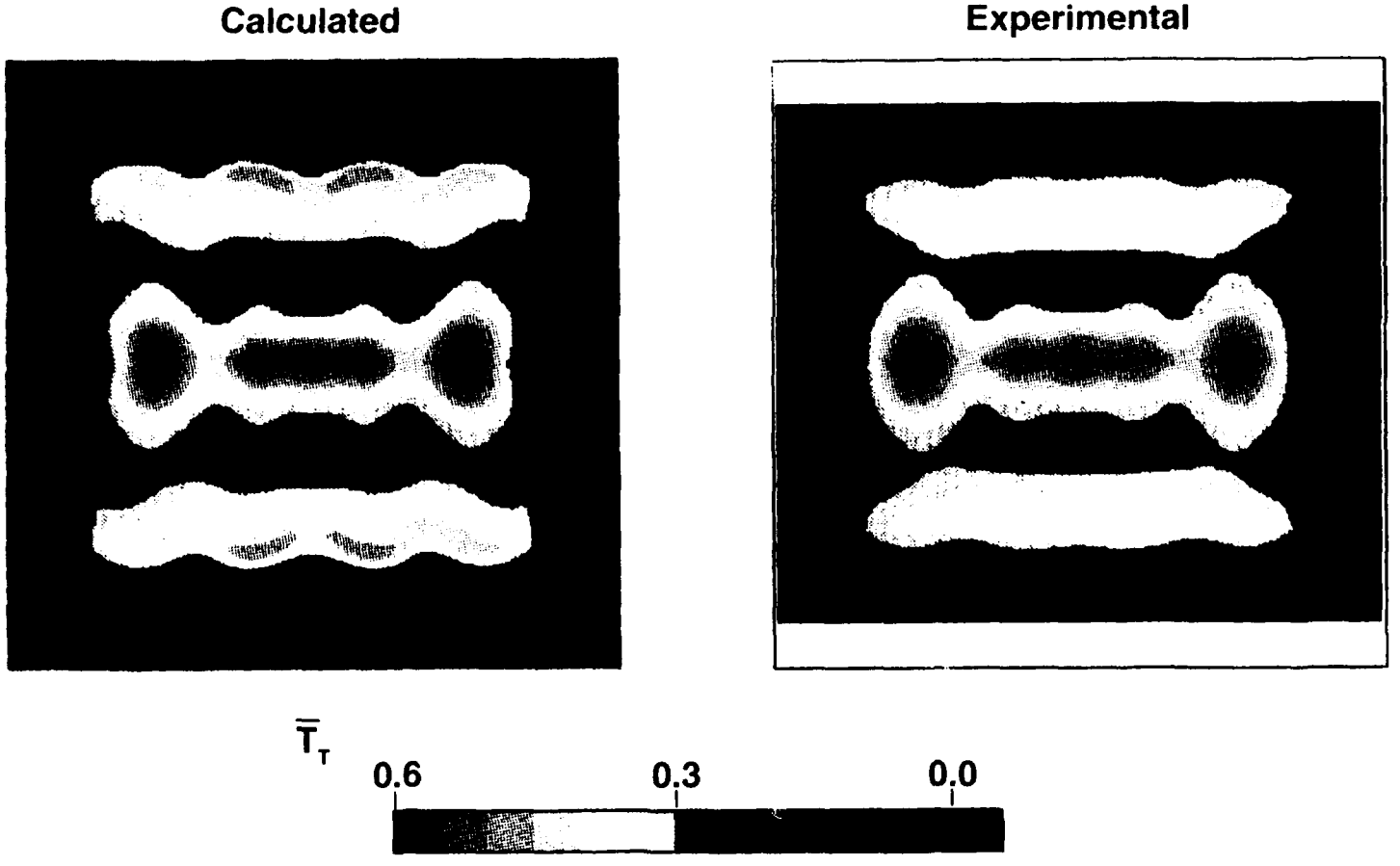

Figure 4

MIXER-EJECTOR: PLUME TOTAL TEMPERATURE: X=10.3 in.
(A_s/A_p=4.0, M_∞=0.5)

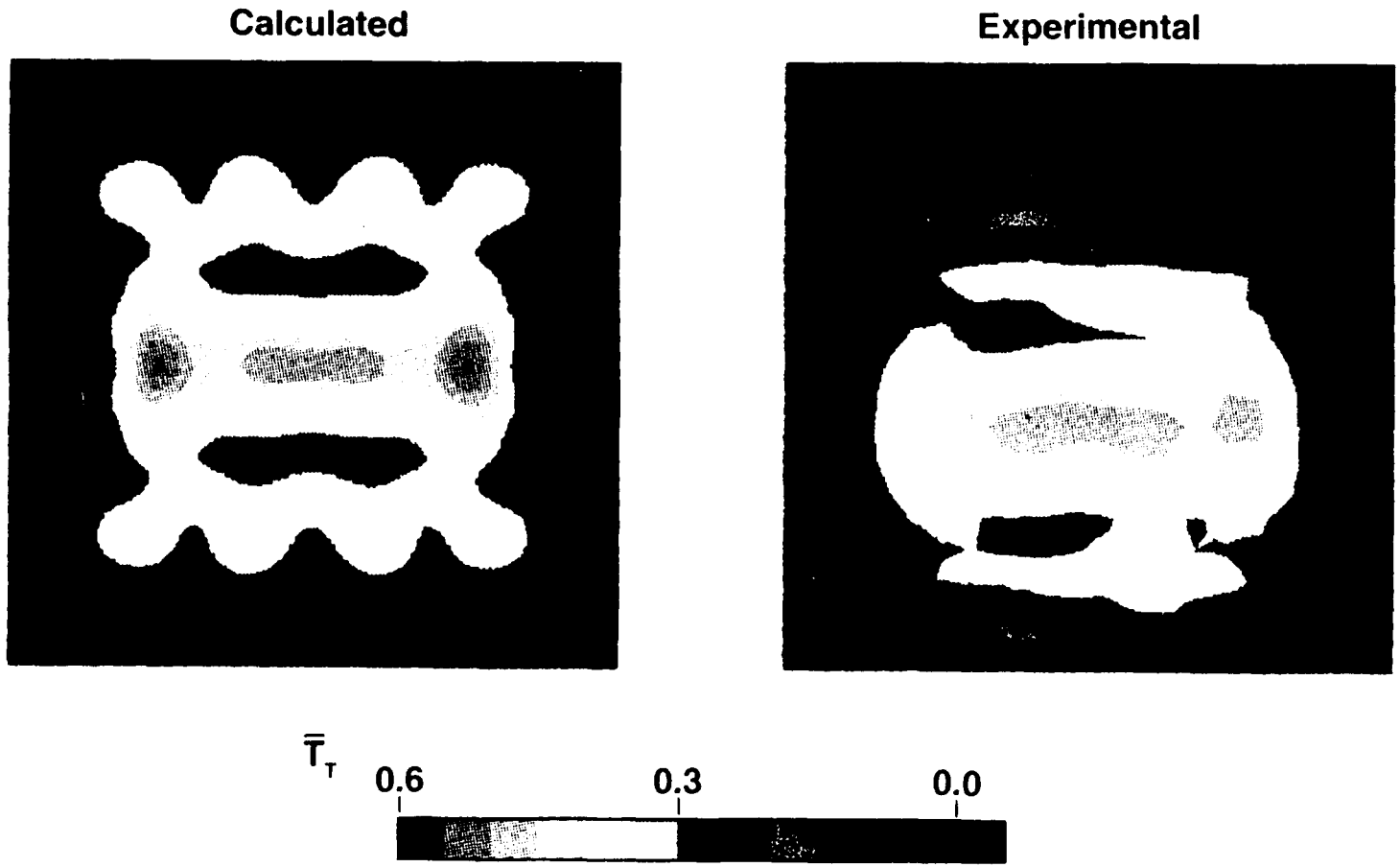

Figure 5

MIXER-EJECTOR: PLUME TOTAL TEMPERATURE: X=40.3 in.
(A_s/A_p=4.0, M =0.5)

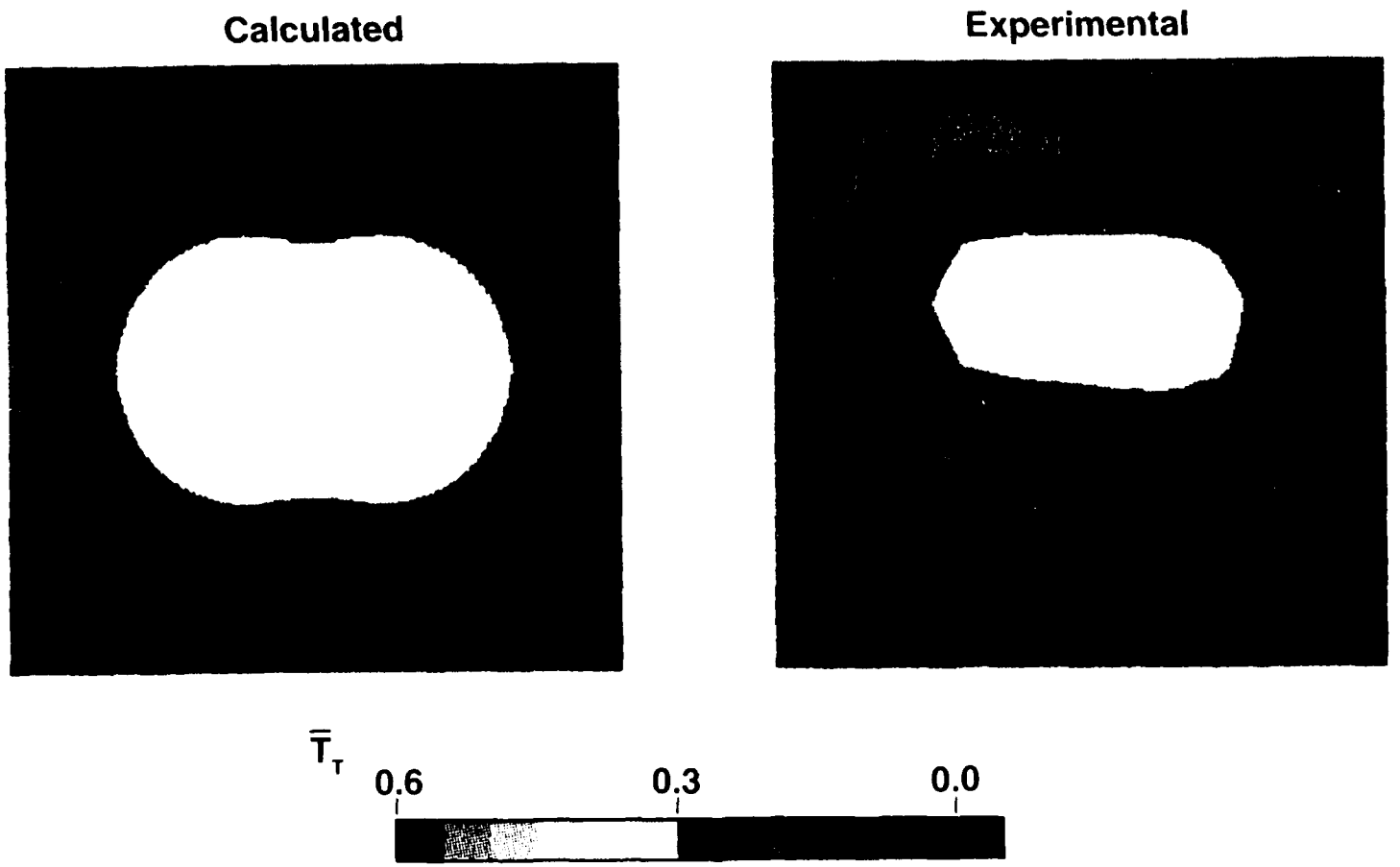

Figure 6

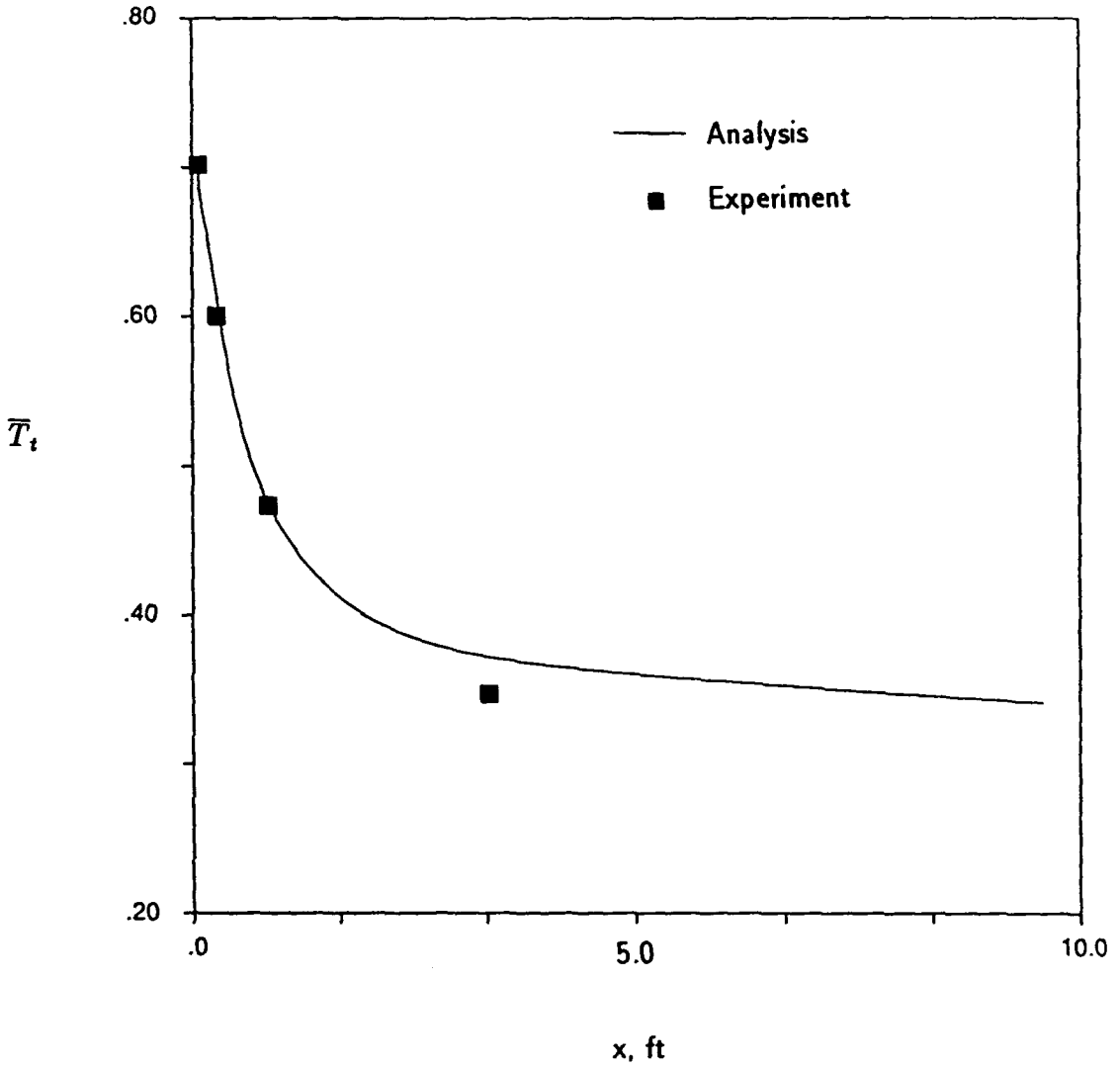

Figure 7: Centerline Total Temperature Decay

EFFECT OF GRID ON PLUME TOTAL TEMPERATURE: X=40.3 in.
(A_S/A_P=4.0, M_∞=0.5)

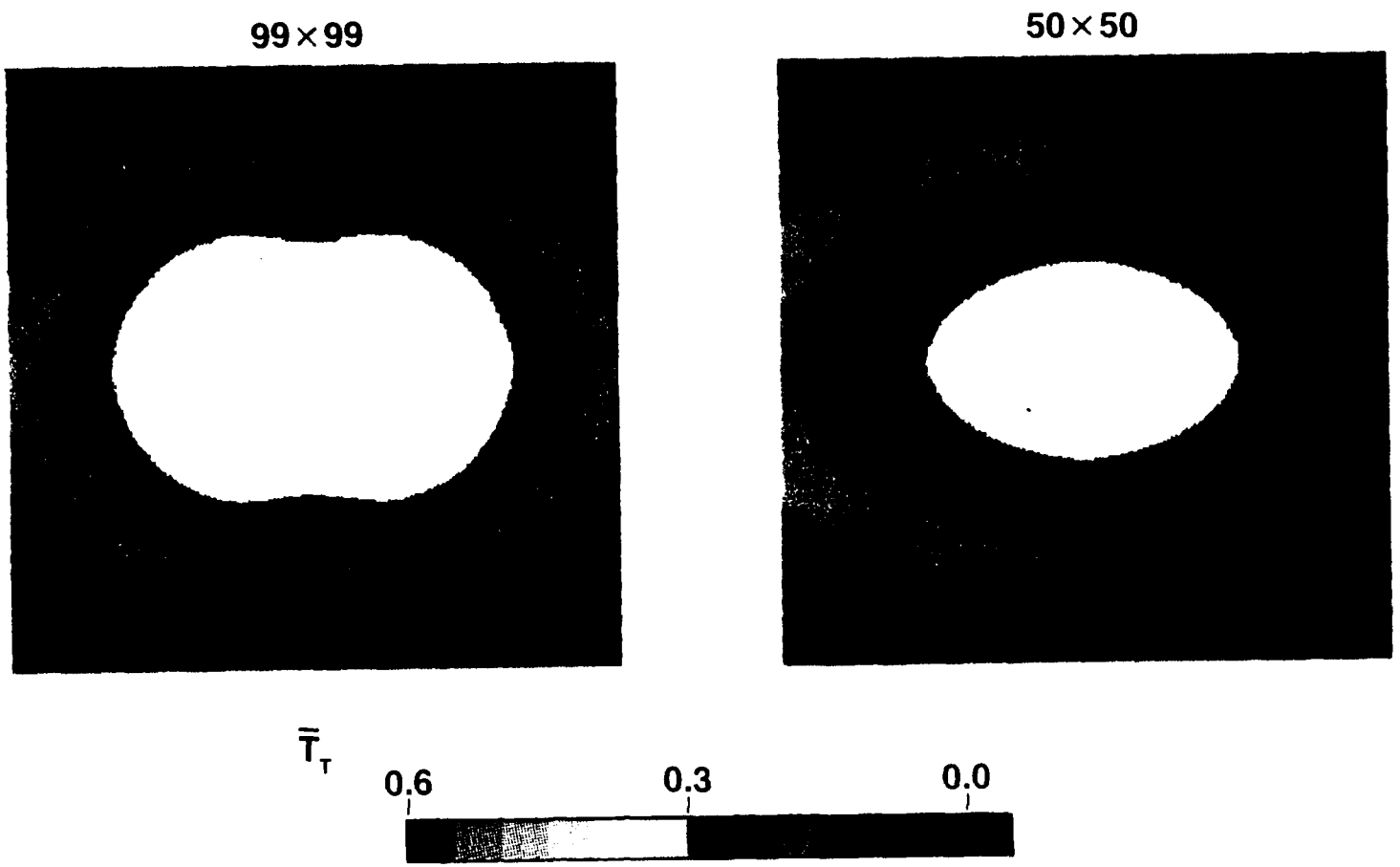

Figure 8

92-2-26-5

EFFECT OF INITIAL TURBULENCE LEVEL ON PLUME TOTAL TEMPERATURE: X=10.3 in. (A_S/A_P=4.0, M_∞=0.5)

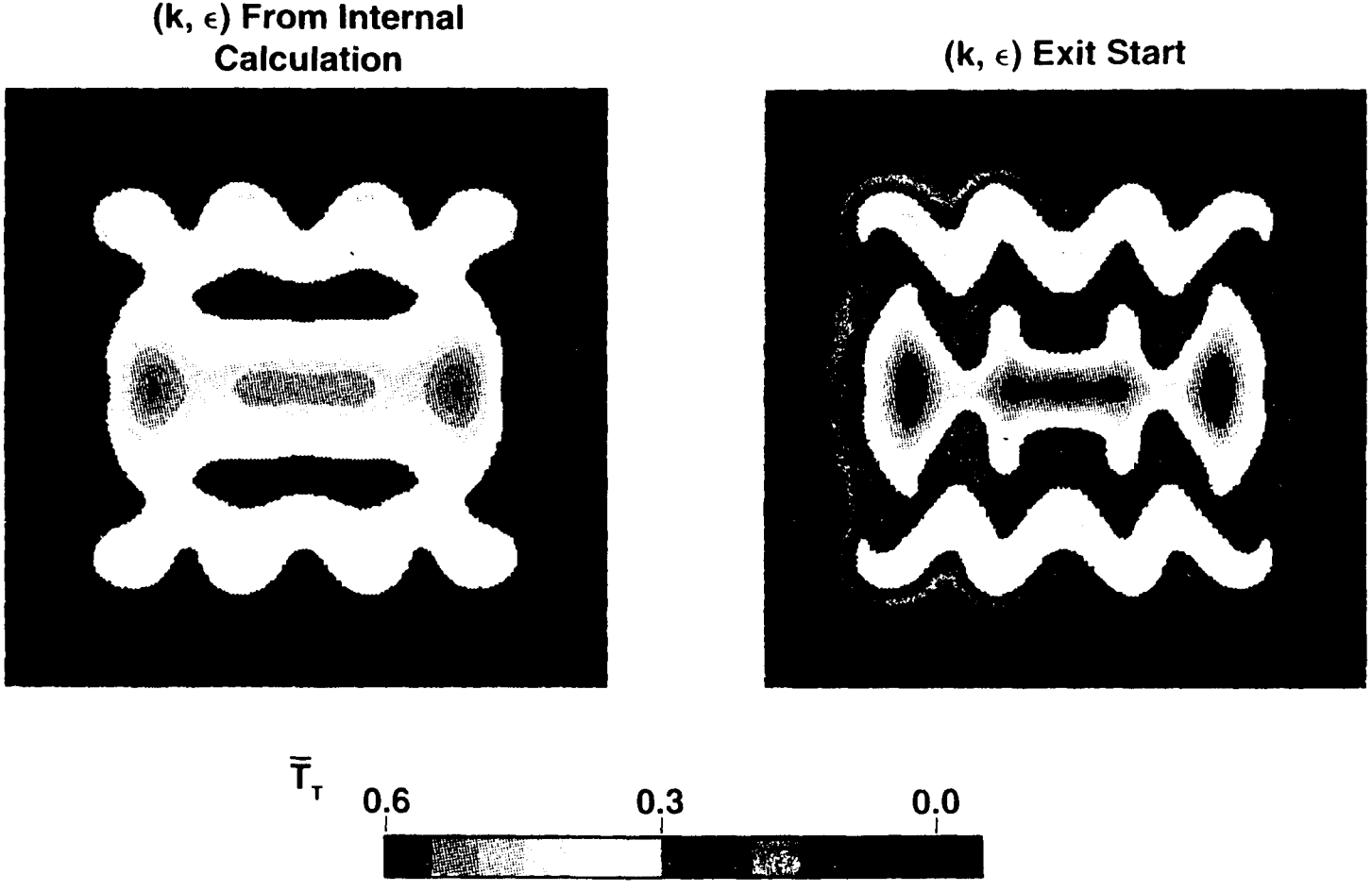

Figure 9

92-2-26-6

EFFECT OF EXIT PLANE VORTICITY ON PLUME TOTAL TEMPERATURE: X=10.3 in. (A_s/A_p=4.0, M_∞=0.5)

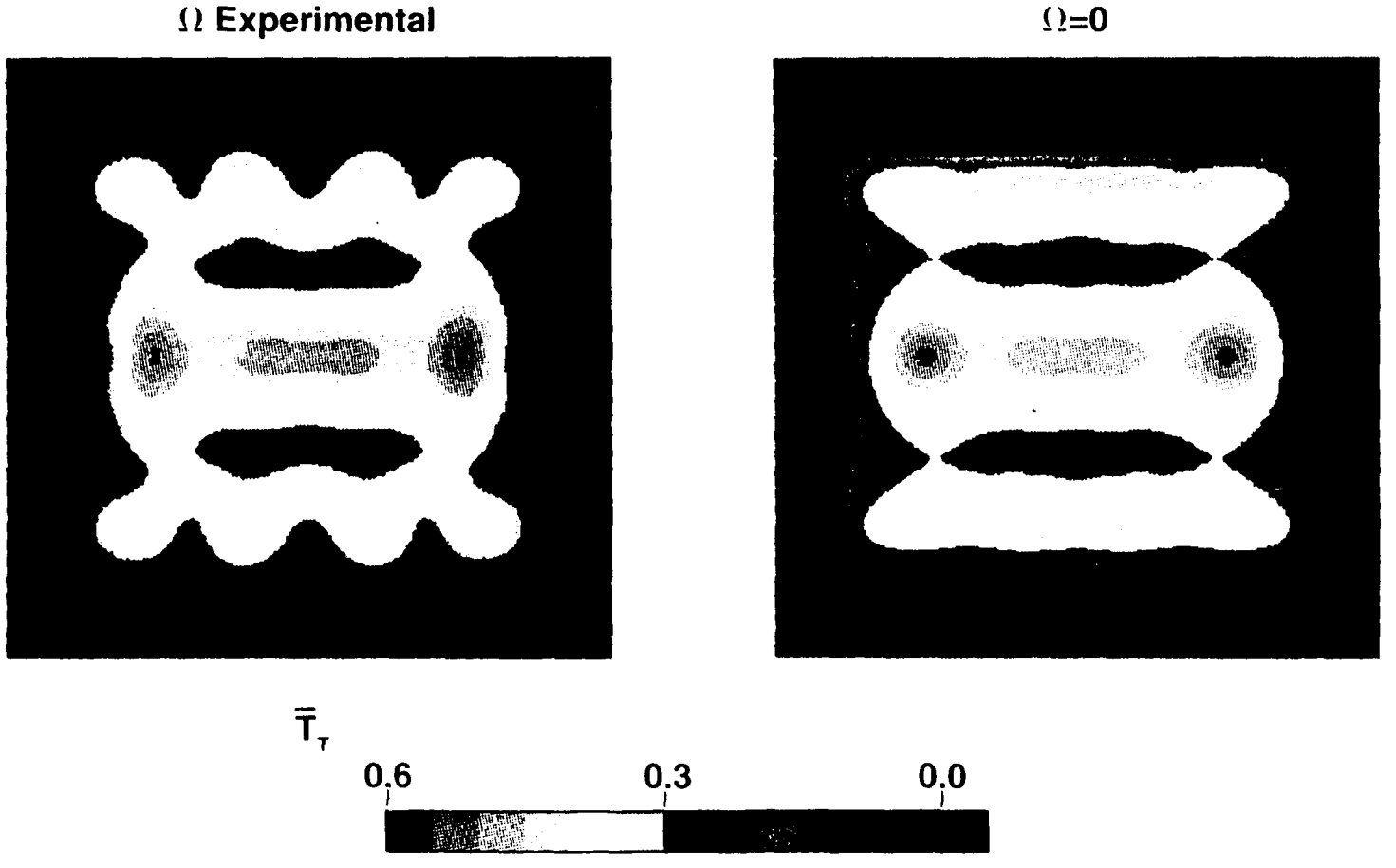

Figure 10

92-2-26-7

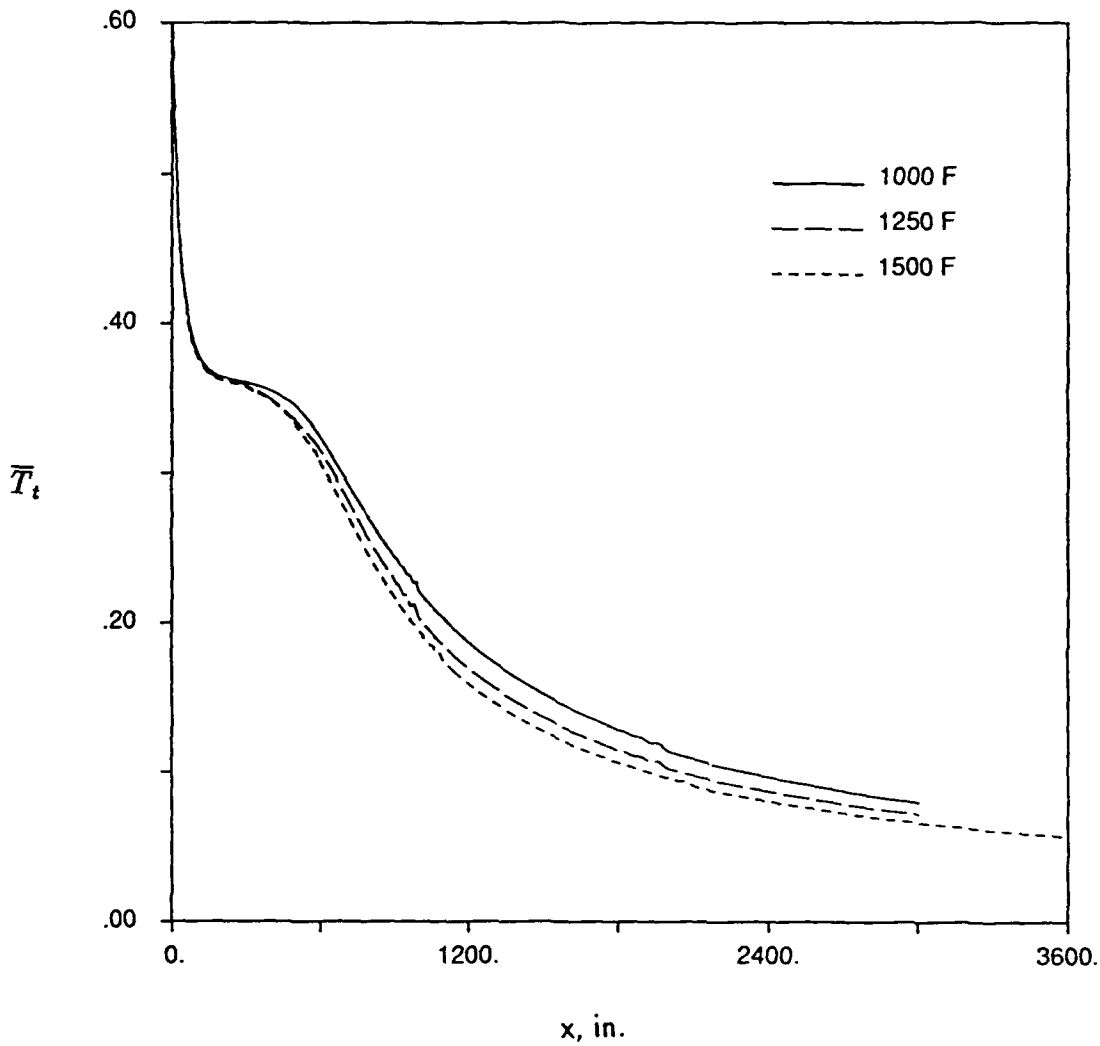

Figure 11: Full-Scale Centerline Total Temperature Decay

PLUME TOTAL TEMPERATURE PLATEAU EFFECT
(A_S/A_P=4.0, M_∞=0.5)

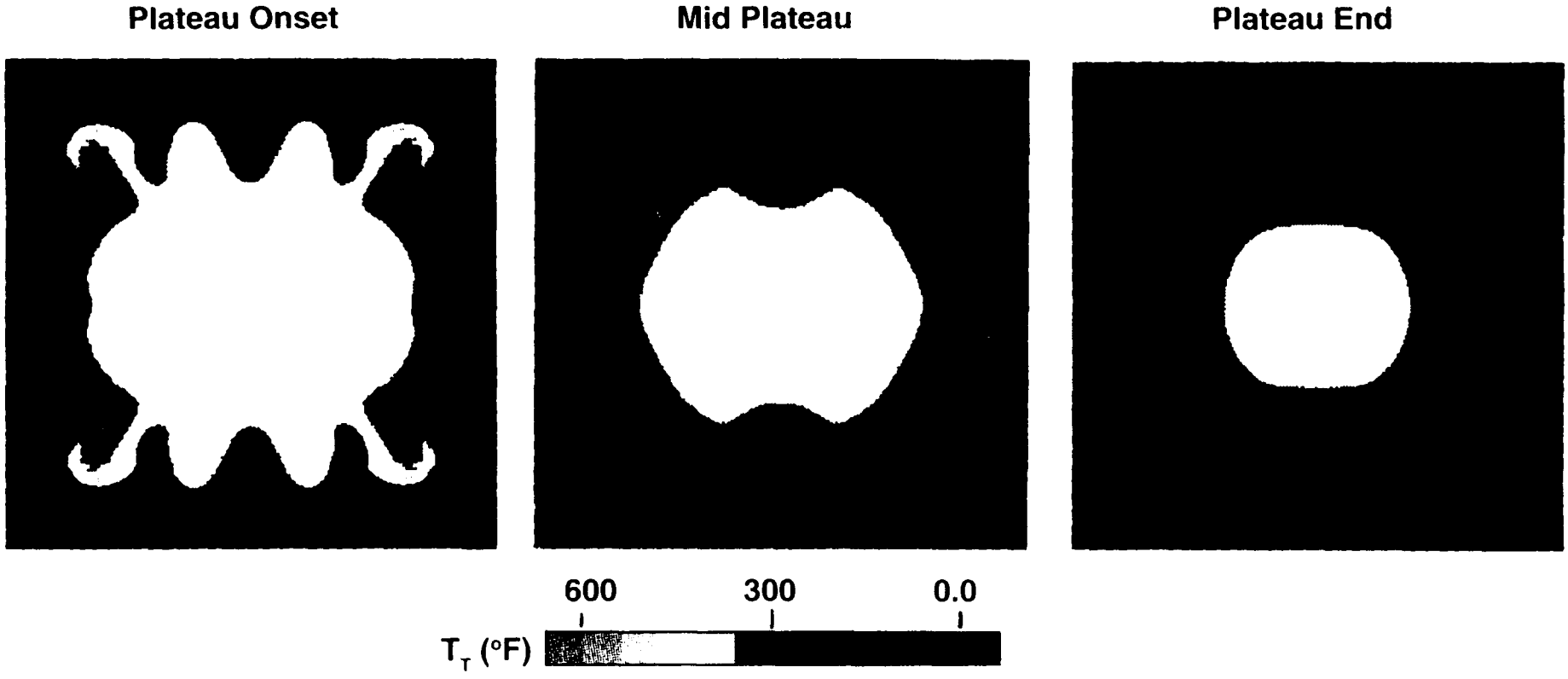

Figure 12

8 Appendix: Ejector Internal Flow Analysis

An internal flow analysis capability has been developed using a combination of CFD (PNS) and empirical data. The computational domain is described in the schematic of the internal portion of the mixer ejector exhaust system showing the end and side view of the ejector respectively (Figs. 1 and 2). It consists of an exhaust nozzle surrounded by a rectangular shrouded duct. The end view, shown in Fig. 1, has an outline of the advanced mixer exhaust nozzle surrounded by a rectangular shroud of width W_E and height H_E. The side view shown on Fig. 2 shows the advanced mixer exhaust nozzle exit plane at $X/L = -1$ surrounded by a shrouded duct of length L. The parameters for the different test geometries which were calculated are shown on Table 1. The tests conducted by Presz and Morin [1] included both the slot nozzle of $AR = 3.0$ and an advanced mixer nozzle with approximately the same exit area.

The flow conditions for all three experimental programs are summarized on Table 2. The Presz and Morin [1] experiment was conducted with a cold primary and a static coflow. The Tillman et al. [2] experiment however was conducted with a hot primary and a coflowing stream having a forward flight Mach number of 0.1.

Initial conditions for this analysis are required at the primary flow nozzle exit plane $X = 0.0$ (see Fig. 2) in order to calculate the flow in the mixer ejector exhaust system. These conditions were not measured in any of the tests cited above. However, experimental data is available from the tests conducted by Patrick et al. [2] for same the slot nozzle and the advanced mixer nozzle operating as free jets. This data consists of normalized total pressure P_T, normalized total temperature T_T, and cross flow velocity components U_2, U_3 *traverses at the nozzle exit plane.* In the report by Patrick et al. [2], a vorticity distribution was determined by estimating the vorticity distribution until the velocity components matched the measured data. This distribution was then used in the present calculations.

Cold Flow Mixer-Ejector Analysis: In our initial validation study, *the cold flow mixer-ejector* configuration of Presz and Morin [1] was examined. In their experiments, measurements of total pressure and Mach number at three stations inside a mixer-ejector and a slot or rectangular nozzle ejector were obtained. Schematic views of the ejector system is shown in Figs. 1 and 2. measurements were taken at duct/primary area ratios (AR) of 3.0, 4.5, 5.2 as shown in Table 1 for the flow conditions given on Table 2.

Comparisons of the measured and calculated total pressure distributions for the slot-nozzle and the advanced mixer nozzle are shown in Figs. 13 through 17 for the three planes marked in Fig. 2. The

Table 1: Mixer-Ejector Geometry

L	$= 10.5\ (in)$
A_{rect}	$= 9.082\ (in^2)$ Slot Nozzle
A_{mixer}	$= 9.164\ (in^2)$ Mixer Nozzle

Case Defin.	M_s	H_E	W_E	AR	A_s/A_p
Cold slot [1]	0.28	4.64	6.04	3.1	2.0
Cold mixer [1]	0.64	4.64	6.04	3.0	1.9
Cold mixer [1]	0.46	6.81	6.01	4.5	3.3
Cold mixer	-	7.86	6.01	5.2	4.2
Hot mixer [2]	0.80	4.64	6.04	3.0	1.9
Hot mixer [2]	0.52	6.81	6.01	4.5	3.3
Hot mixer [2]	0.37	7.86	6.01	5.1	4.0

Table 2: Flow Conditions for Mixer-Ejector Cases

Reference	Presz & Morin	Tillman et al.
M_∞	0.0	0.1
P_{TJ} *psia*	51.60	49.61
$P_{T\infty}$ *psia*	15.23	15.23
$T_{TJ}\ ^\circ R$	500.00	1460.00
$T_{T\infty}\ ^\circ R$	500.00	501.00

slot nozzle predictions shown in Fig. 17 agree remarkably well with the experimental observation. These observations, when compared to previous isolated slot nozzle experiments and calculations, demonstrate that the nozzle shear layer growth is largely unaffected by the ejector pumping, resulting in little mixing of the jet flow with the freestream. The color contour comparisons for the mixer-ejector combination are shown in Figs. 14 through 15. These figures show reasonable agreement with experimental data, matching the mixing process both in structure and level. Note that the central core feature is retained substantially longer than the lobe features. This is largely due to the lack of penetration of the induced secondary flow and will be explored in more detail shortly. A quantitative comparison of the calculated and measured total pressures is shown in Figs. 16 and

17 for the advanced mixer nozzle ($AR = 3.0$). The total pressure comparisons show the calculation to be in generally good agreement with the experimental measurements. These figures show comparisons at the initial and exit plane for the slices at the center plane $Z = 0.0$ and off the center plane at $Z = 0.15$ which indicate quite good agreement as to general level and distribution.

The mixing effectiveness parameters E_m, E_T, E_H have been calculated for the slot nozzle and mixer nozzle cases, showing that, for this cold flow condition, $E_m = E_T = E_H$. Furthermore, the slot nozzle has a mixing effectiveness of only 34% while the mixer nozzle has an improved mixing effectiveness of about 60% for the equivalent ejector area ratios.

The development of the secondary flow or streamwise vorticity field (quarter plane only) is shown in Fig. 18 for the $AR = 3.0$ and $AR = 4.5$ mixer ejectors. At station $X/L = -1.0$, the vorticity field is similar to the free jet. The plots show the vorticity concentrated along the shear layer with + or - values aligned to the mixer lobe sidewalls. Note that for the $AR = 3.0$ mixer ejector, the tip of the lobes are very close to the upper wall. At $X/L = -0.5$, the $AR = 3.0$ ejector has developed a very strong vortex compared to the $AR = 4.5$ ejector which is centered between the outer lobes. By $X/L = 0.0$, much of this vortex has been dissipated. One should note the low level of outward flow from the central or core nozzle flow. The presence of crossflow stagnation points, where the centerline intersects the lobe bisector, can be seen as the mechanism for producing the four "bulls-eye" regions seen in Figs. 14 and 15. These results differ from the free jet results reported in Ref. [2] in that the strong vortex does not develop. A more objective measure of the secondary flow mixing is the absolute circulation given by,

$$|\Gamma| = \oint |\Omega| ds \tag{7}$$

and the average value of the vorticity given by

$$\bar{\Omega} = \frac{|\Gamma|}{A} \tag{8}$$

which are plotted in Figs. 19 and 20. At $X/L = -1.0$, the circulation is the same for all area ratios. It can be seen in Figs. 19 that for the $AR = 3.0$ where the tip of the lobe is very close to the wall, the absolute value of the circulation reaches peak values much higher than for the other cases. On the other hand, from Fig. 20 it can be seen that the average vorticity decreases with increasing area ratio. While each calculation starts with the same level of circulation, the effect of AR produces a greater effect on the average vorticity. This behavior was graphically seen in Fig. 18.

Table 3: Hot Flow Mixer Ejector Percent Mixing

AR	4.48	5.21
E_m	60.	54.
E_T	55.	50.
E_H	56.	51.

Hot Flow Mixer-Ejector Analysis: Additional code validation was obtained in hot flow mixer-ejector comparisons with the data of Tillman et al. [2]. In their experimental studies, total temperature profiles were measured at the ejector exit plane for duct / primary area ratios (AR) of 3.0, 4.5, 5.1. The specific flow conditions for these cases are given on Table 2. Initial plane conditions at the primary nozzle exit plane ($X/L = -1.0$) were obtained from the data contained in a report by Patrick et al. [2].

Comparisons of the measured and calculated total temperatures at the mixer ejector exit plane are shown in Figs. 21 through 24. In Figure 21, it can be seen from the experimental data that the mixing patterns previously seen in the cold flow cases is still present. The effect of the heated jet has raised increased the total pressure drop and resulted in a partial mixing of the hot exhaust flow. Again the most prevalent structure at the exit plane is the residual effect of the nozzle core flow. The effect of increased area ratio (AR) results in greater ejector pumping. This is seen at the exit plane in Fig. 21 and along the centerline (from nozzle exit to the farfield) in Fig. 22. The axial length has been normalized by d, the diameter of a round nozzle having an equivalent exit area to the mixer nozzle. At the ejector exit, the temperature ratio has drop almost 50%. Similar centerline decay results have been previously reported for mixer-type nozzles, however in this ejector configuration, the overall exit plane temperature level has been reduced from that observed in the isolated mixer nozzle case. It should be noted that while one frequently assesses a jet's mixing performance in terms of it's centerline history, such three-dimensional configurations exhibit flow nonuniformities off of the centerline. In such cases, the integrated mixing parameters Eqns (11) - (13) or the cross plane plots represent better measures of mixing. Detailed comparisons of measured and calculated total temperature are shown in Figs. 23 and 24. In addition, for these cases the degree of mixing for both area ratios are shown in Table 3. The degree of mixing appears to decrease with increasing area ratio for the two area ratios indicated in Table 3.

References

[1] Presz, W. M., and Morin, B. L., "Supersonic Mixer-Ejector Program," UTRC Report UTRC89-19, July 1989.

[2] Tillman, T. G., Paterson, R. W. and Presz, W. M.. " Supersonic Nozzle Mixer Ejector," AIAA Paper AIAA-89-2925, AIAA 25th Joint Annual Propulsion Conference, July 1989.

[3] Tillman, T. G., Patrick, W. P., Paterson, R. W., "Enhanced Mixing of Supersonic Jets," AIAA 88-3002, AIAA 24th Joint Propulsion Conference, July, 1988.

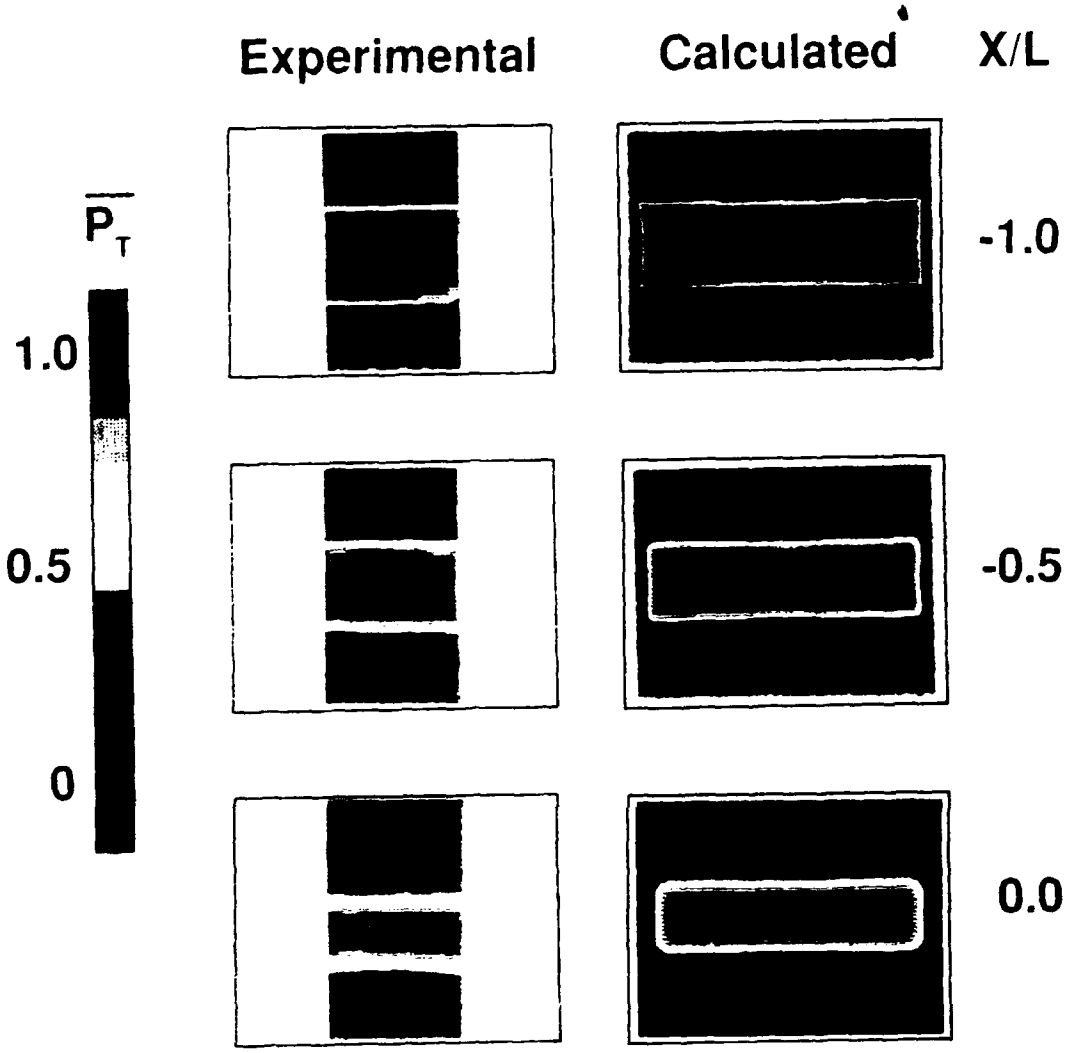

Figure 13: *$\overline{P}_t$ Distributions for a Supersonic Slot-Nozzle Ejector: $AR = 3.0$*

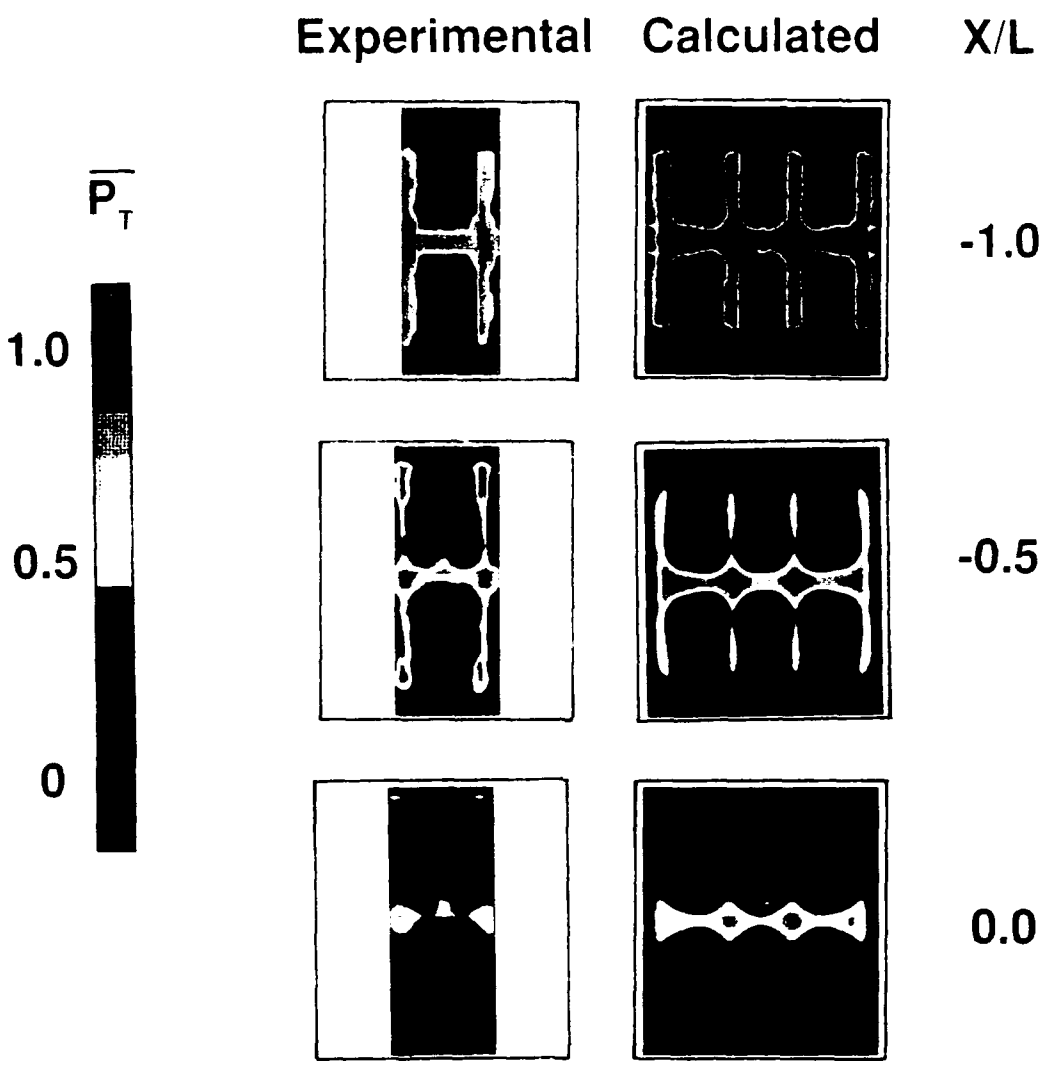

Figure 14: *$\overline{P}_t$ Distributions for a Supersonic Mixer-Ejector: AR = 3.0*

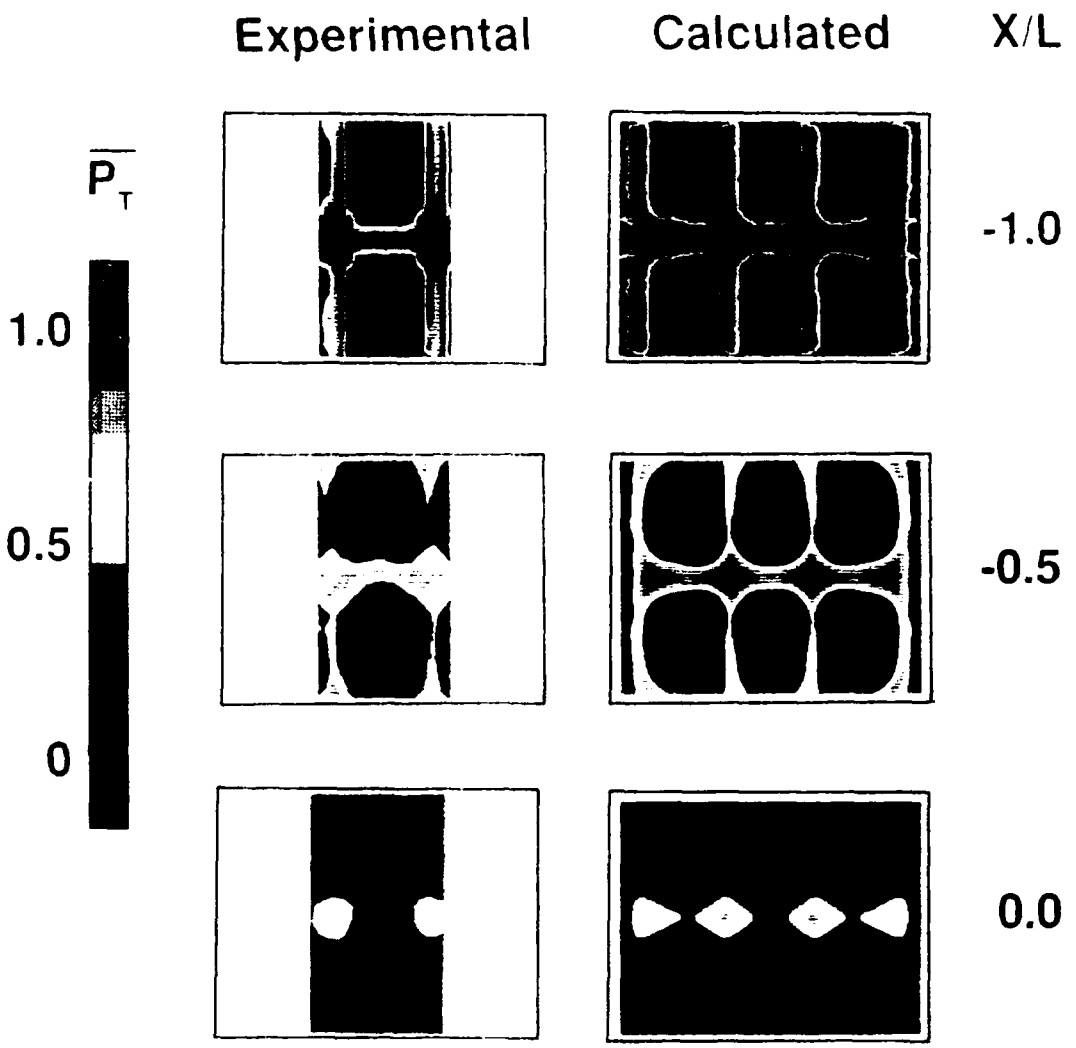

Figure 15: *$\overline{P}_t$ Distributions for Supersonic Mixer-Ejector: AR = 4.5*

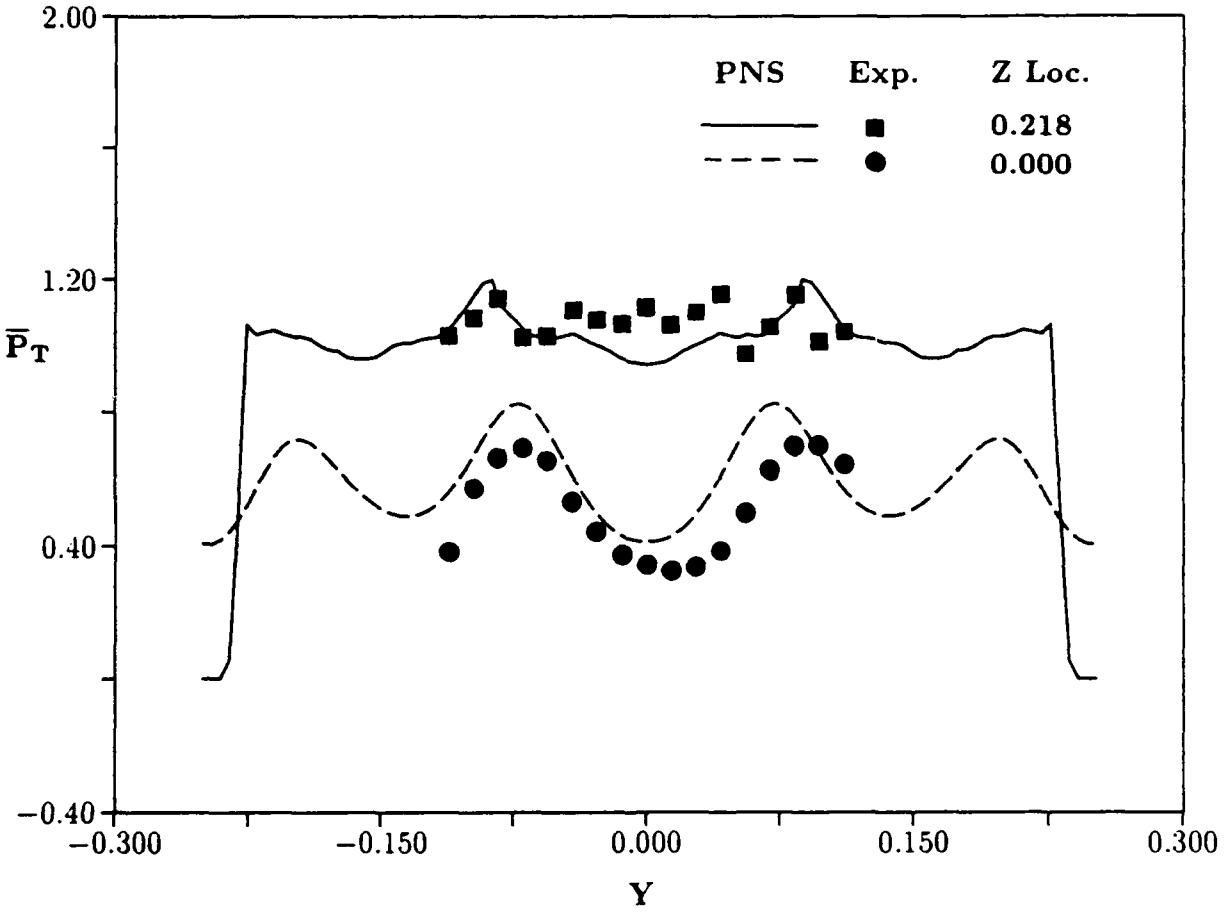

Figure 16: *Measured and Calculated $\overline{P}_T$ In a Supersonic $AR = 3.0$ Mixer-Ejector at $Z = 0.00ft$*

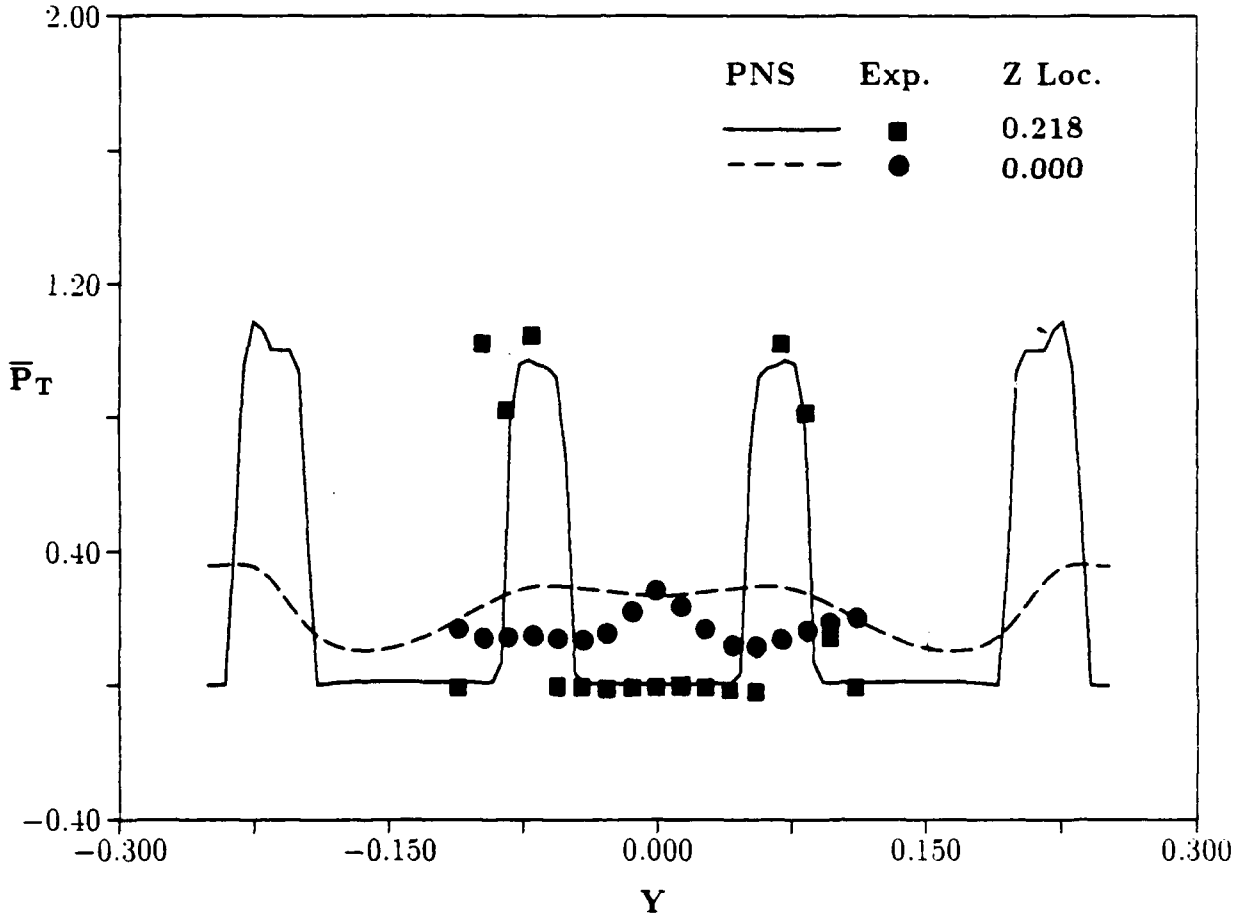

Figure 17: *Measured and Calculated $\overline{P}_T$ In a Supersonic AR = 3.0 Mixer-Ejector at Z = 0.15ft*

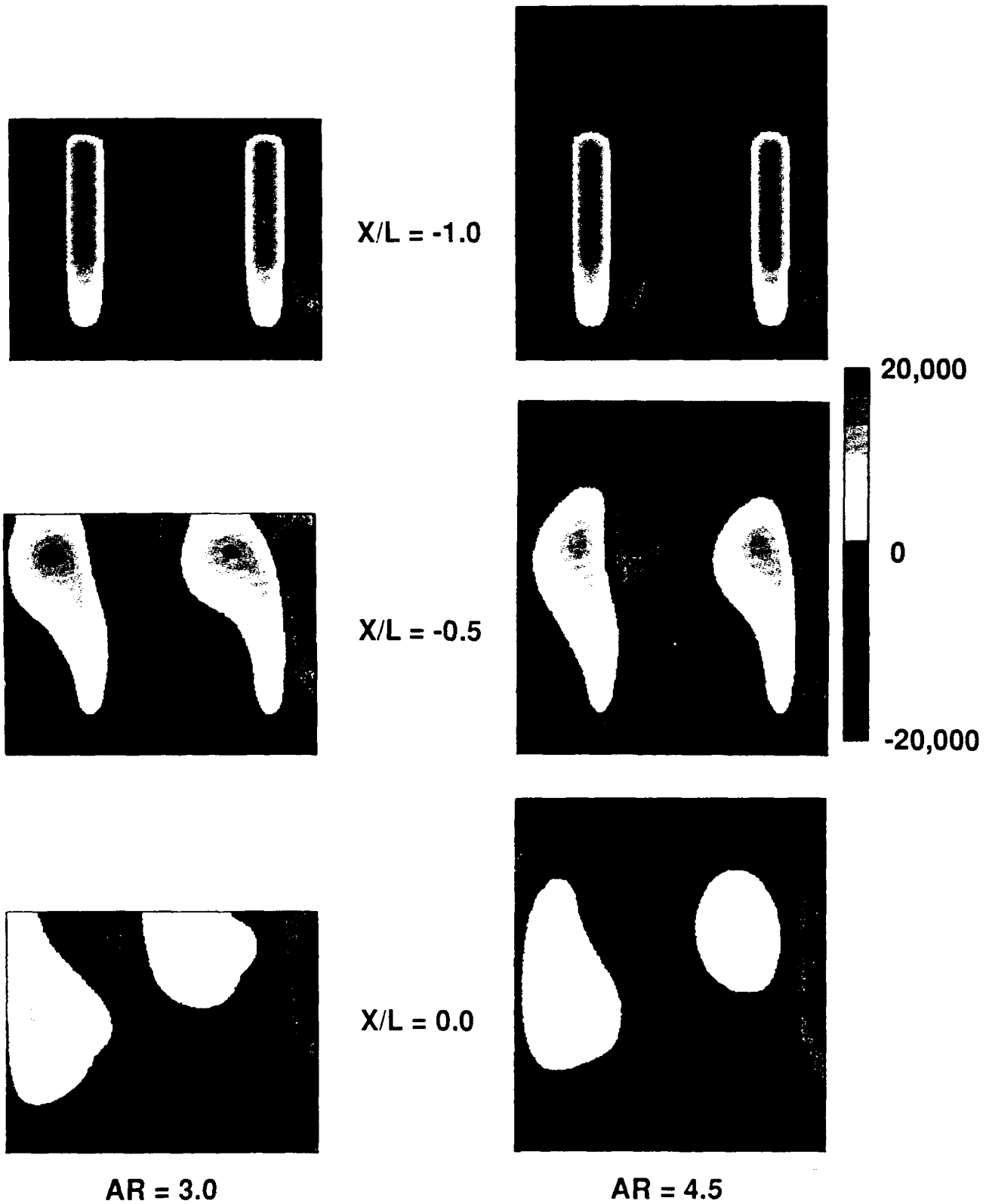

Figure 18: *Comparison of Streamwise Vorticity Fields in Supersonic Mixer-Ejector*

91-10-56-5

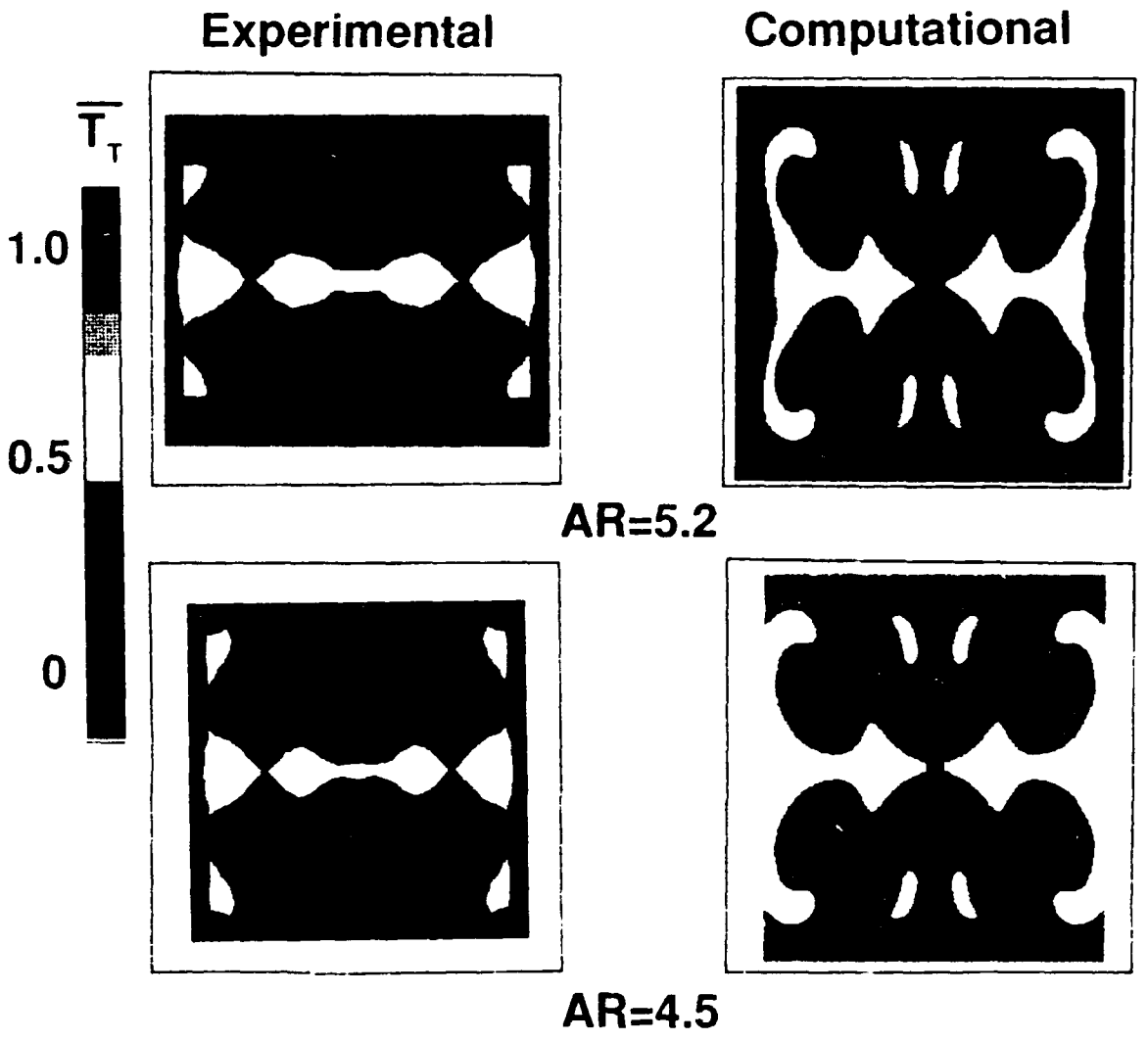

Figure 19: *Calculated and Measured $\overline{T}_T$ Distributions for Hot Flow Supersonic Mixer-Ejectors*

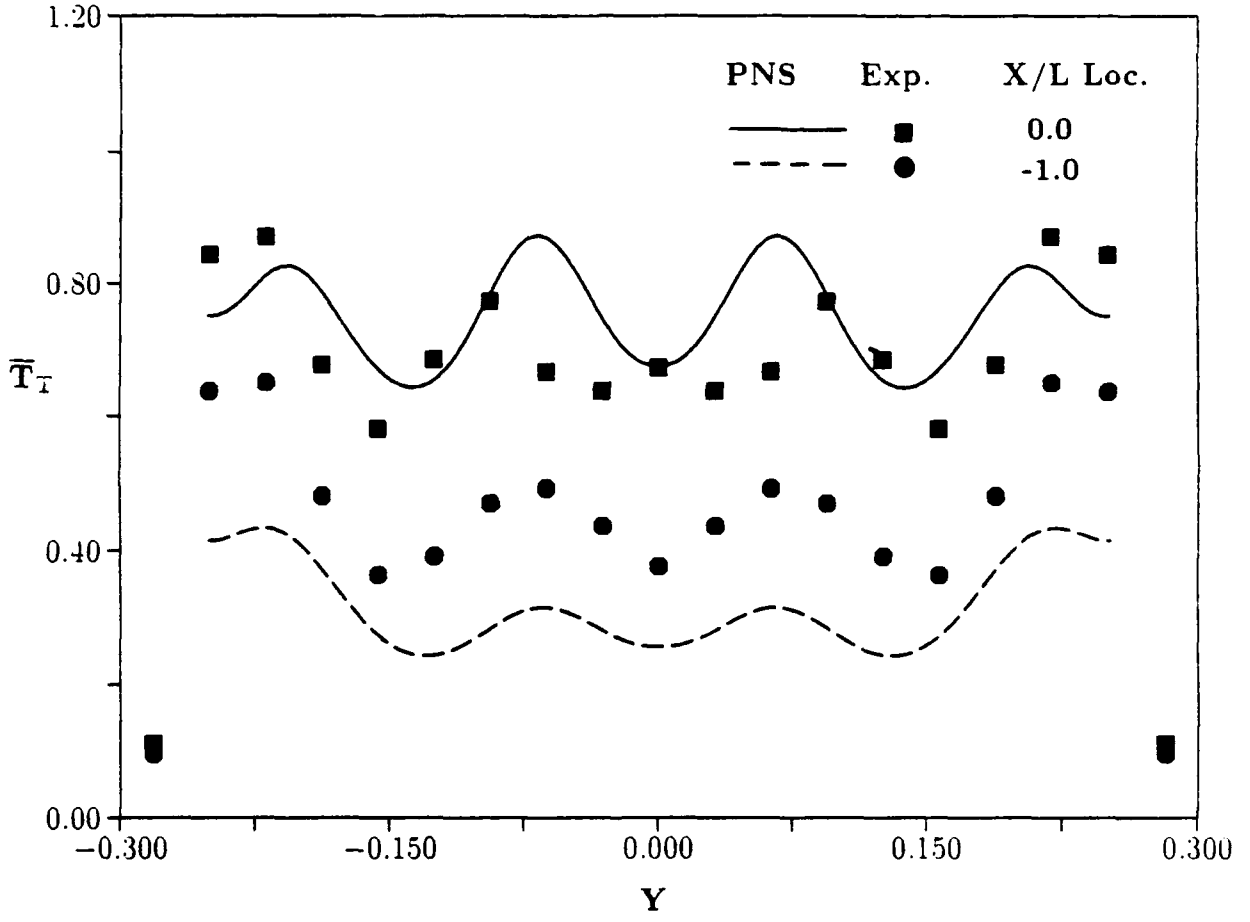

Figure 20: *Measured and Calculated Exit Plane $\overline{T}_T$ for Supersonic AR = 4.5 Mixer-Ejector*

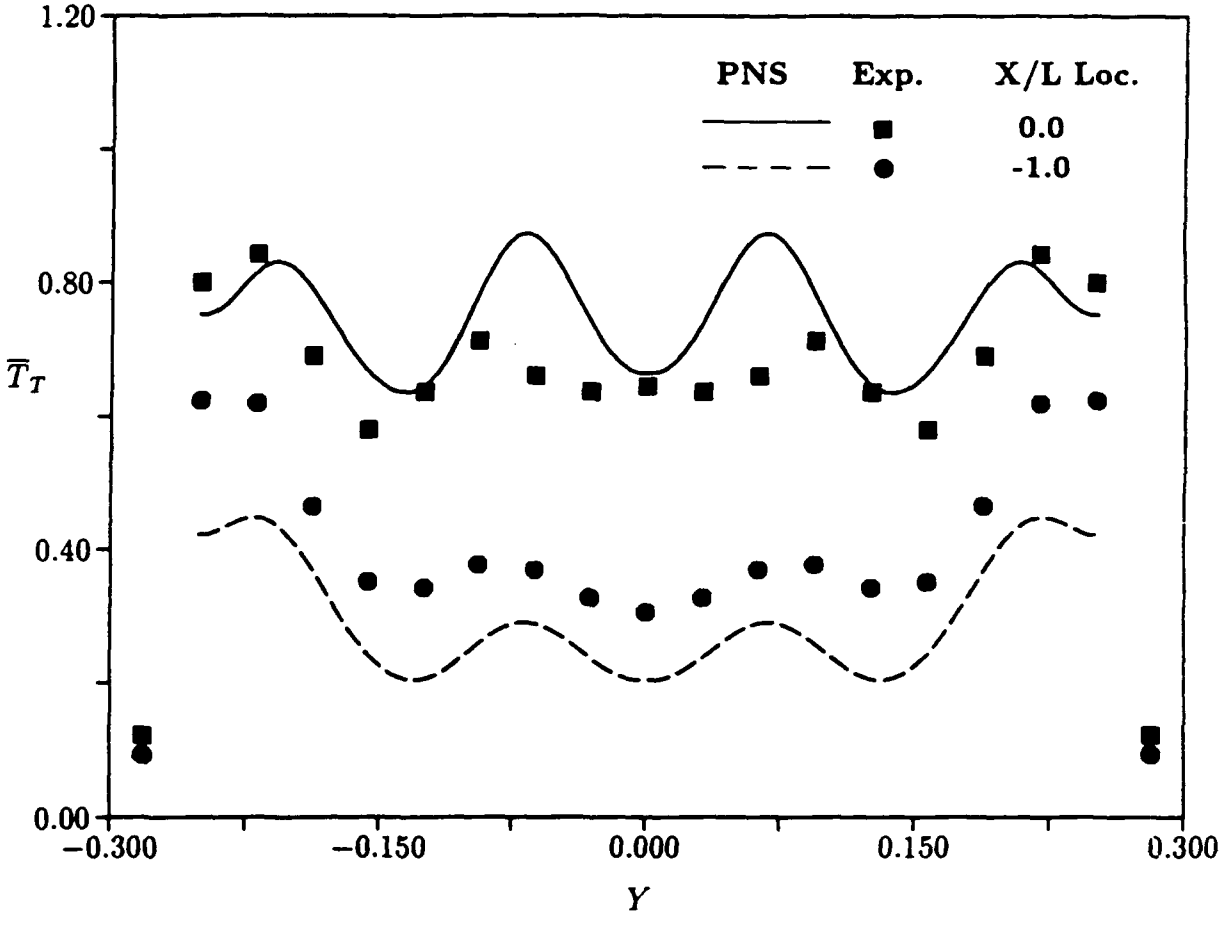

Figure 21: *Measured and Calculated Exit Plane $\overline{T}_T$ for Supersonic AR = 5.1 Mixer Ejector*